A Density Functional Theory Investigation of the Reaction of Water with Ce$_2$O$^-$

Hassan Harb and Hrant P. Hratchian[*]

Department of Chemistry and Biochemistry & Center for Chemical Computation and Theory, University of California, Merced, Merced, California 95343, USA

E-mail: hhratchian@ucmerced.edu

Abstract

Cerium suboxide clusters are a recent catalyst class that has received interest for the generation of H_2 from water. Using density functional theory calculations, this work examines the reaction of Ce_2O^- clusters with H_2O. It is shown that the reaction can proceed along both doublet and quartet pathways. In both cases, hydrogen formation is facilitated by intermediate structures featuring bridging hydride and hydroxide ligands. Interestingly, it is shown that metal d electrons facilitate the reduction of water. This work provides new understanding of this reaction and provides new insight into the reactivity of small lanthanide-based clusters with water.

1   Introduction

Water, being one of the most abundant substances in nature, has been the subject of intense interest for scientists to study its physical and chemical properties.[1–11] In addition to the roles water plays in myriad chemical reactions and biological systems, H_2O has been a key focus in energy related research. Of particular interest are catalysts facilitating the four-electron $2H_2O \longrightarrow 2H_2 + O_2$ reaction.[12–17] Cerium oxides attracted special interest recently due to their ability to efficiently catalyze a wide range of oxidation and reduction reactions, including water-gas shift reactions.[18–22] Several studies have also shown that cerium oxide-supported metal surfaces exhibit increased catalytic activity relative to their non-cerium oxide supported analogues.[23–35]

Surface defects due to metal or oxide deficiencies possess unique electronic properties and facilitate increased reactivity. Such defect sites exhibit incomplete valencies and localized electronic structures.[36] As with other metal oxides, the catalytic activity of lanthanide oxide surfaces is most active at surface defect sites. However, studying extended surfaces is complicated by the low concentration of surface defects and the continuous structural changes along the surfaces. Alternatively, small gas-phase lanthanide oxide clusters can serve as representative model systems for studying reactivity of defect sites on extended surfaces.

Several experimental and computational studies have been performed on cerium oxide clusters in order to better understand the electronic structure features that pave the way to a thorough understanding of their reactivity and catalytic activity. In addition, various experimental and theoretical studies have explored the reactivity of classes of cerium-based clusters with various gas-phase small molecules.[17,19,37–51] Of particular interest here are computational studies conducted by Zhou and co-workers on the reactivity of Ce_n (n=1-3) with up to six water molecules.[37,38] Their results indicate high reactivity of these cerium clusters and their efficiency in decomposing multiple water molecules. Recently, Jarrold and co-workers reported mass spectra of $Ce_xO_y^-$ systems (x= 2,3 ,y= 1-4) and their products from reactions of the clusters with water.[17] Their results indicate that cerium oxide clusters undergo three types of reactions: hydrogen gas production, water abstraction, and hydroxide abstraction. The relative selectivity of one reaction type over the others is highly dependent on the stoichiometry of the cluster. For example, Ce_2O^-, Ce_3^-, $Ce_3O_2^-$, and $Ce_3O_2^-$ preferentially produce H_2 gas, while clusters with equal stoichiometric ratios of Ce and O undergo OH abstraction, and clusters bearing more oxide than cerium ions undergo water abstraction.

In this work, we consider the simplest stoichiometric cluster of cerium oxide capable of efficient H_2 gas production, Ce_2O^-. Previously reported experimental results include data from mass-spectrometry and photoelectron spectroscopy, which provide valuable information on the geometric and electronic structures of the studied molecules.[17,48] With those results in mind, we first examine the geometric and electronic structure of different clusters potentially involved in the reaction. We then explore the potential energy surfaces corresponding to various states and identify a likely pathway for H_2 formation from water at Ce_2O^- clusters.

2 Computational Methods

Calculations were performed using a development version of the GAUSSIAN suite of electronic structure programs.[52] The B3PW91 density functional was employed.[53–57] The unrestricted formalism was used for all calculations.[58,59] The stability of all calculated Kohn-Sham determinants was verified.[60–62] The Stuttgart relativistic small core atomic natural orbital basis set and corresponding effective core potential (ANO/ECP) basis set with 28 core electrons and a contracted valence basis set (14s13p10d8f6g)[6s6p5d4f3g] was used for cerium center.[63] The Dunning style correlation-consistent basis set aug-cc-pVTZ was used for oxygen and hydrogen centers.[64,65]

Geometry optimizations were carried out using standard methods and the nature of each located potential energy surface stationary point was confirmed by vibrational frequency analysis.[66] Intrinsic reaction coordinate (IRC) calculations were performed to ensure that optimized transition structures connect appropriate potential energy surface minima.[67,68] Reported enthalpies of reactions were calculated at $298\,\mathrm{K}$. Relative energies including zero-point corrections at $0\,\mathrm{K}$ are reported in the supporting information.

We note that systems featuring multiple metal centers and open-shell electronic structure, such as those studied here, can potentially exhibit multi-reference character. For this reason, the results from DFT calculations must be interpreted with some caution. The approach used here follows from our previous experience working with such systems as well as studies reported by other groups.[46,47,51,69–75]

3 Results

In the discussion that follows, structures are labeled as *X-n*, where *X=A,B,C...* represents a particular molecular structure and the value of *n* indicates the multiplicity of the cluster. For example, **A-4** refers to the quartet spin state of structure **A**. Transition structures are labeled as **TS1-***n* and **TS2-***n*. Again, *n* denotes the spin multiplicity of the transition

structure. A thorough search for numerous isomers and electronic states was performed to identify candidate reactants, intermediates, products, and transition structures.

As discussed in greater detail below, this investigation ultimately identified two viable pathways for the reaction $Ce_2O + H_2O \longrightarrow Ce_2O_2 + H_2$. Specifically, it was found that reactions along doublet and quartet pathways are both likely. In both cases, the reaction begins water addition to a Ce_2O anion cluster, followed by formation of hydride and then hydroxide bridges, and finally yields evolution of molecular hydrogen (Scheme 1).
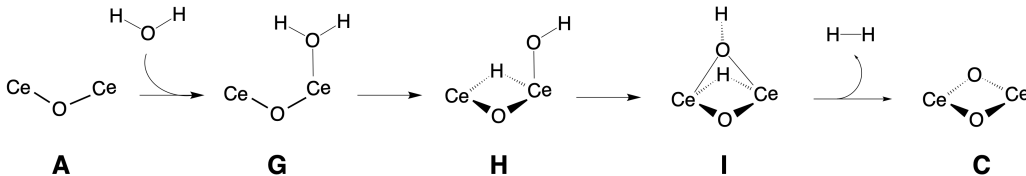
Scheme 1: Overview of the proposed mechanism for the reaction $Ce_2O + H_2O \longrightarrow Ce_2O_2 + H_2$.

3.1 Reactant and Product Cerium Oxide Clusters

Prior to exploring the mechanism of $Ce_2O^- + H_2O \longrightarrow Ce_2O_2^- + H_2$, we considered possible structures of the initial Ce_2O^- cluster species and the final oxidized cluster $Ce_2O_2^-$. Various molecular structures and electronic configurations were considered. For the Ce_2O^- molecular cluster, two general structural motifs are possible: (1) the oxygen atom can bridge the two cerium atoms (Compound **A**, Fig. 1); or (2) the oxygen can be in a terminal position and bound to only one cerium site as only (Compound **B**, Fig. 1). In addition to the molecular structure, we examined multiple spin-states. Specifically, calculations were carried out on the doublet, (ground-state) quartet, and sextet multiplicities.

Our calculations showed that several different structures of Ce_2O^- species exist. Figure 1 shows the energetically competitive Ce_2O^- species. The ground state of Ce_2O^-, **A-4**, is a quartet state featuring a bridging oxide. In this structure, the two $Ce-O$ bonds are equivalent with a bond length of 2.06 Å and a $Ce-O-Ce$ angle of 120.8°. The sextet **A-6** lies 3.92 kcal/mol higher than **A-4** and the doublet state **A-2** is only 2.1 kcal/mol higher in

energy than the ground state. These results are in agreement with the anion photoelectron spectroscopy results published by Kafader et *al.*[47]

Another located structure, **B-6**, features a terminal oxide and has a sextet spin ground state. This structure is much higher in energy than the others, at 48.40 kcal/mol higher than **A-4**. Quartet and doublet states were not found for structure **B**. Despite its absence in the previously reported photoelectron spectrum of Ce_2O^- [47] and its higher energy relative to the ground-state **A-2**, we still considered the possibility of the role of **B-6** in the reaction with water and consequent H_2 production. Nevertheless, we were unable to locate a reaction pathway starting with **B-6** and leading to the evolution of H_2.
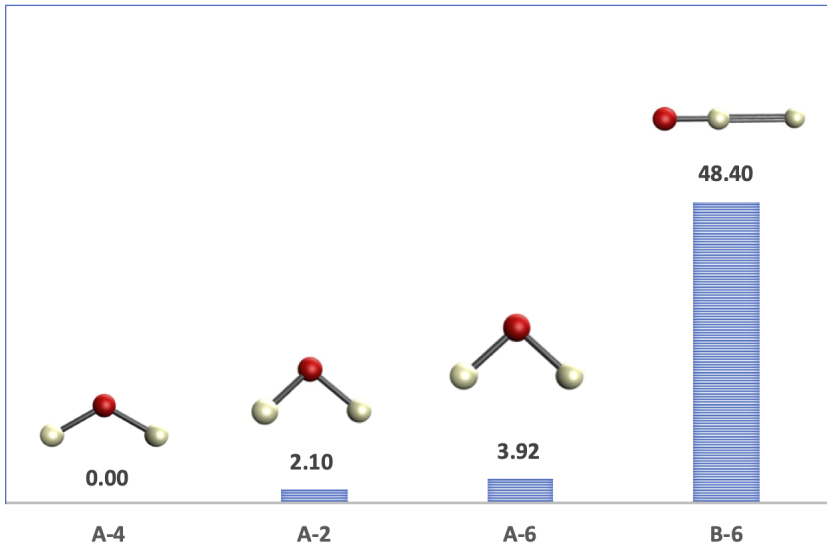

Figure 1: Optimized structures and energies of located Ce_2O^- clusters. Energies are given in kcal/mol and are relative to that of **A-4**.

We next considered candidates for the product $Ce_2O_2^-$ clusters. As for the initial cluster species **A** and **B**, each oxide in the product cluster can either be at terminal or bridging positions. We found four different general geometric structures; considering doublet, quartet, and sextet spin states resulting in 11 distinct candidate final product clusters, which are shown with their relative energies in Fig. 2.

The ground state produce cluster, **C-4**, is a quartet planar compound with both oxygens bridging the two cerium ions. Another closely lying state is doublet **C-2**, which has a

geometry similar to the ground-state. **C-2** lies only 0.63 kcal/mol higher than **C-4**, and the geometries of the two structures are quite similar.

Compounds **C-6** and **F-2** lie approximately 25 kcal/mol higher in energy than **C-2** and **C-4**. Sextet **C-6** is 24.94 kcal/mol higher in energy than **C-4**. Although the structure of **C-6** is similar to **C-4** and **C-2**, **C-6** is not a planar structure. Specifically, the Ce−O−Ce−O torsion angle is 20.3°, unlike **C-4** and **C-2** that are planar.

An additional set of higher energy $Ce_2O_2^-$ isomers (**D**, **E**, and **F**) were also located. The geometry of **F-2**, which is close in energy to **C-6** at 27.14 kcal/mol relative to the lowest-energy **C-4** cluster, is quite different. Specifically, one oxide is terminal while the other one is bridging. Given that **D-2**, **D-4**, **D-6**, **E-2**, **E-4**, **E-6**, and **F-6** are all much higher in energy (58.73 - 162.47 kcal/mol) we presume that they do not contribute to the mechanistic study presented in this paper and do not consider them further.
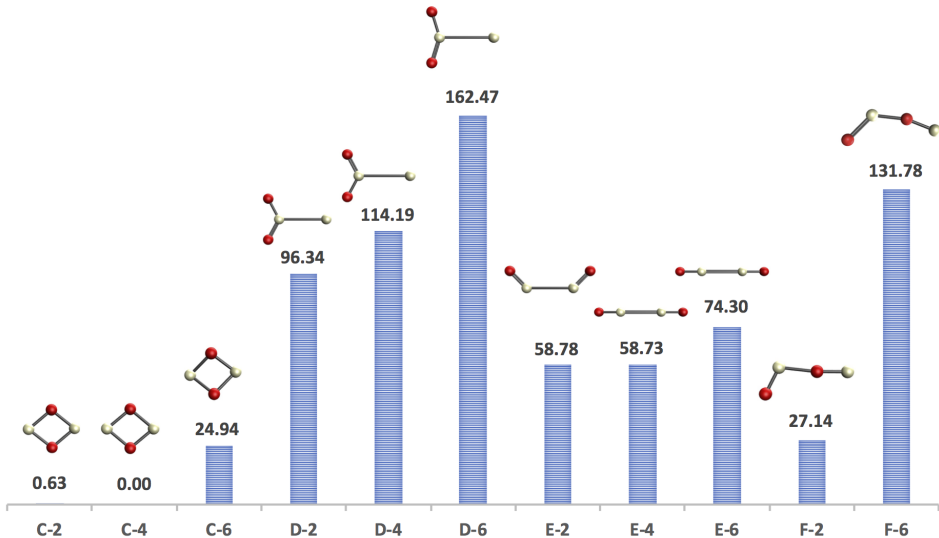

Figure 2: Optimized structures and energies of located $Ce_2O_2^-$ clusters. Energies are given in kcal/mol and are relative to that of **C-4**.

In previous work, Kafader et al. reported the anion photoelectron spectra of Ce_2O^- and $Ce_2O_2^-$ together with a computational analysis to fully characterize the observed structures.[47] DFT calculations and Franck-Condon simulations were used to determine that the

ground-state configuration of Ce_2O^- is a $^4A_2$ state with the $Ce-O-Ce$ bridge bonding being the favored structural motif, resulting in C_{2v} symmetry. They found another close-lying $^2A_2$ state with a bonding motif resembling the ground-state quartet species. These two structures correspond to **A-2** and **A-4** structures reported in this work (Fig. 1). Using the same approach, Kafader et al. determined the ground-state configuration for $Ce_2O_2^-$ to be a ^4A_g state with the ^2A_g state being slightly higher in energy. Both structures exhibit D_{2h} symmetry and Franck-condon simulations confirmed their contributions to the photoelectron spectrum. These two structures resemble **C-4** and **C-2** shown in Fig. 2, respectively. As far as the starting materials and the final products are concerned, our computational results are in good agreement with the results reported by Kafader and coworkers. Thus, the two (non-relativistic) potential energy surfaces to be explored are the $^4A_2$ and $^2A_2$ routes that start with compounds **A-4** and **A-2** and lead to ^4A_g and ^2A_g clusters **C-4** and **C-2**.
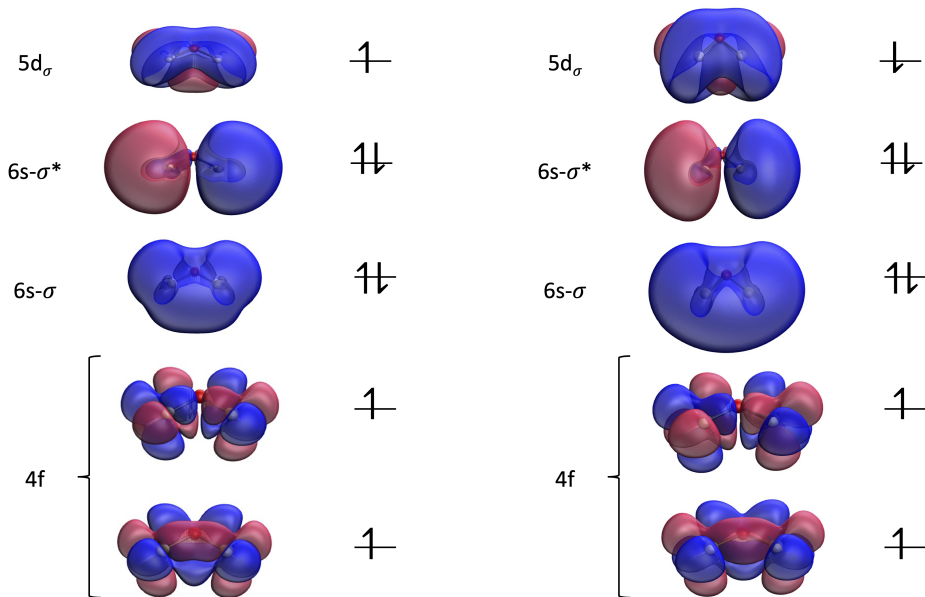

Figure 3: Valence molecular orbitals of quartet (left) and doublet (right) Ce_2O^-

Figure 3 shows the frontier molecular orbitals (MOs) of **A-2** and **A-4**. The MO diagram of **A-4** is comprised of three general manifolds: 4f, σ/σ^*, and 5d orbitals. The first frontier orbital group includes two singly occupied 4f orbitals localized on the cerium centers. The σ and σ^* orbitals are doubly occupied and are predominantly Ce 6s-based. Finally, the highest

occupied MO (HOMO) of quartet Ce_2O^- **A-4**, is a 5d-based singly occupied orbital with the electron delocalized across the two cerium centers. Similar to **A-4**, the frontier MOs for **A-2** feature doubly-occupied $6s_\sigma$ and $6s_\sigma^*$, and singly-occupied $5d_\sigma$ β orbital and 4f orbitals. The difference between the MO diagrams of **A-4** and **A-1** is the spin of the occupied $5d_\sigma$ orbital.

MO diagrams for **C-2** and **C-4** (shown in Fig. 4) exhibit more similarity to each other than **A-2** and **A-4**. Both spin states of structure **C** include the two singly occupied 4f orbitals present in their respective starting **A** clusters. In addition, both doublet and quartet spin states have a doubly occupied 6s-based σ orbital and a singly occupied σ^* orbital. The only difference is the spin of the electron occupying the σ^* orbital. The quartet has an α electron in the σ^* orbital, while that same orbital is occupied by a β electron in the doublet **C-2**. In a manner similar to the reactants, the doublet and quartet $Ce_2O_2^-$ differ in the spin of the singly-occupied $6s_\sigma^*$ orbital.

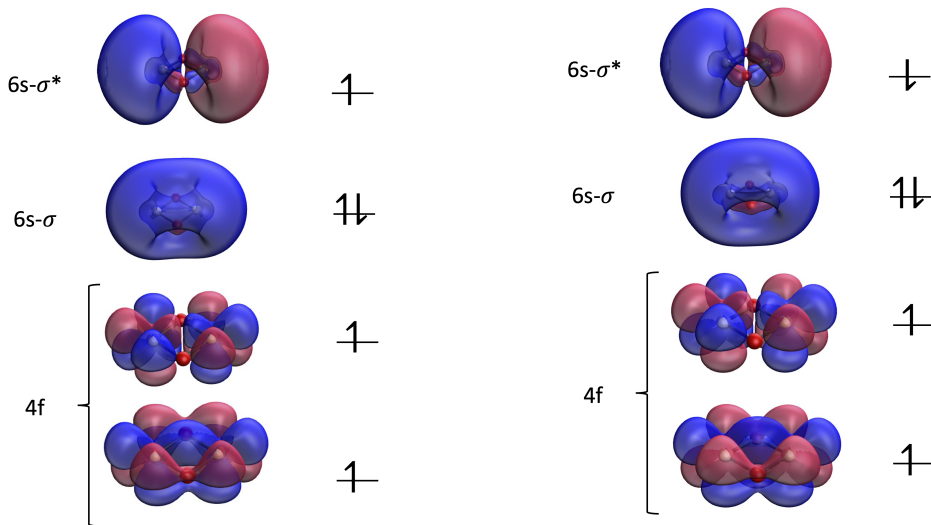Figure 4: Valence molecular orbitals of quartet (left) and doublet (right) $Ce_2O_2^-$

The combined oxidation state of the two cerium centers is (+I) in Ce_2O^- and (+III) in $Ce_2O_2^-$. Figures 3 and 4 show that the frontier molecular orbitals of both Ce_2O^- and $Ce_2O_2^-$ exhibit delocalization of electrons over the two cerium metals. In addition, as discussed in the previous sections, all Ce−O bonds are equivalent within the same molecule in both the

Ce_2O^- and $Ce_2O_2^-$. For these reasons, the oxidation states of the cerium centers should also be equal. Furthermore, given the delocalized nature of the frontier orbitals over the two cerium centers we take our computational results to suggest two resonance structures that have cerium centers with unequal oxidation states. For Ce_2O^-, the studied structure can be described by two resonance structures of Ce_2O^-, with each resonance form featuring one Ce(0) and one Ce(I) center. In a similar manner, the final $Ce_2O_2^-$ structures **C-4** and **C-2** are described by two Ce(I)/Ce(II) resonance structures.

3.2   Water Addition

The reaction of Ce_2O^- with water begins with water addition. We have identified one unique mode for water addition to clusters **A-2** and **A-4**. This mode is best described as an interaction between the water oxygen and a terminal cerium atom, while the second cerium atom does not directly engage in this step. Water addition to the Ce_2O^- clusters **A-2** and **A-4** forms structures **G-2** and **G-4**. A notable feature about both adduct structures is that a water hydrogen is oriented towards the distant cerium, suggesting the feasibility of hydrogen interaction with the remote cerium center.
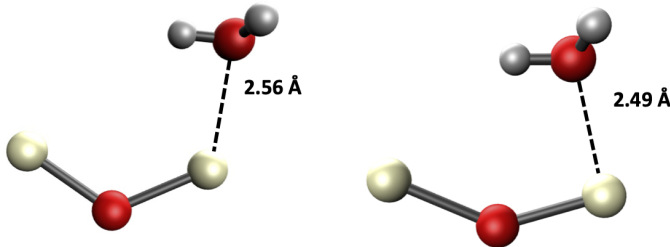

Figure 5: Quartet G-4 (left) and doublet G-2 (right) with intermolecular distances given in Angstroms.

The relative heats of reactions of the water adducts are shown in Fig. 5. Formations of both adducts resulting from water addition to Ce_2O^- are exothermic, with ΔH values of -13.0 and -12.2 kcal/mol for the doublet and quartet states, respectively. For the formed intermediates, the distance between the water oxygen center and the cerium atom is 2.56 Å

(**G-4**) and 2.49 Å (**G-2**). Additionally, the bound water is oriented such that a hydrogen atom is oriented toward the other cerium center.

3.3 Hydride Bridge Formation

Following water addition, the reaction undergoes Ce oxidation as a water O−H bond is cleaved and leads to formation of a bridging hydride. Structures **H-2** and **H-4** correspond to the resulting intermediates, $Ce_2HO(OH)^-$, that form from O−H bond cleavage in **G-2** and **G-4**, respectively. Figure 6 shows the structure and relative energies of two identified spin states that correspond to structure **H**.

The structure of **H-2** and **H-4** is best described as a four-member planar ring consisting of two cerium atoms, an oxygen, and a hydrogen, with a bound hydroxide ligand. The oxygen and hydrogen centers in the ring are both in bridging positions relative to the two cerium atoms. The bridging hydride binds to the Ce centers with bond lengths of 2.29 Å and 2.30 Å for both the doublet and quartet species. The O−H bond cleavage in both the quartet and doublet states is exothermic with heats of reaction of -73.0 kcal/mol (quartet state, **G-4** $\longrightarrow$ **H-4**) and -73.9 kcal/mol (doublet, **G-2** $\longrightarrow$ **H-2**) relative to their respective starting materials. Such exothermicity suggests the formation of **H-2** and **H-4** is highly thermodynamically favorable.

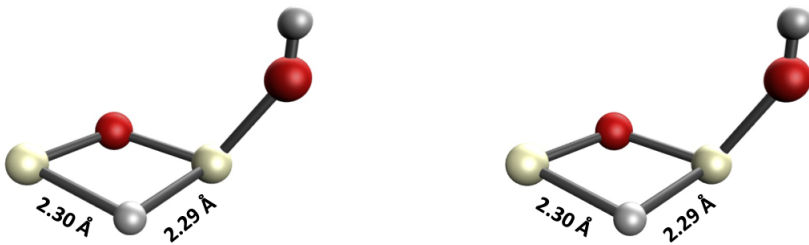
Figure 6: Structures of quartet H-4 and doublet H-2, Ce−O distances are shown in units of Angstroms.

Transition structures **TS1** connect **G** to **H** (Fig. 7). The two transition structures (**TS1-4** and **TS1-2**) are geometrically similar to their respective reactants **G-4** and **G-2**, with the

Figure 7: Structure TS1-4 that connects G-4 and H-4 (left) and TS1-2 that connects G-2 and H-2 (right).

water hydrogen oriented towards the two cerium centers. The Ce−H bond distances are 2.34 Å and 2.80 Å (**TS1-4**) and 2.38 Å and 2.79 Å (**TS1-2**), respectively. Both **G** $\longrightarrow$ **H** reaction steps are essentially barrieless. The **TS1-4** and **TS1-2** energy barriers are only 0.6 kcal/mol (-11.6 kcal/mol relative to **A-4** + H_2O) and 0.2 kcal/mol relative to **G-4** and **G-2** (-11.2 kcal/mol relative to **A-4** + H_2O).

3.4   Hydroxide Bridge Formation and H_2 Production

The relative positions of the two hydrogen centers is critical for the final H_2 formation step. With this in mind, we explored a series of possible rearrangement steps. Our calculations identified **I-2** and **I-4**, both of which feature molecular orientations that are reasonable structural precursors to H_2 formation (Fig. 8). Structures **I-2** and **I-4** include a new hydroxide bridge between the cerium centers, resulting in the two hydrogens being in close proximity to one another (H−H distance is $\sim$ 3 Å). These structures directly lead to subsequent release of H_2 and formation of product clusters **C-2** and **C-4**. By comparing the Ce−H bond lengths of structures **H-2** and **H-4** with **I-2** and **I-4**, we observe a decrease in bond distance as the hydroxide binds to the second cerium atom. Thus, the bond formation between the hydroxide and cerium plays a role in decreasing the distance between one of the cerium atoms and the hydride.

Our calculations identified transition structures connecting **H-2** and **H-4** to **I-2** and **I-4**, shown in Fig. 9. In both cases, the transition structures present small reaction barriers
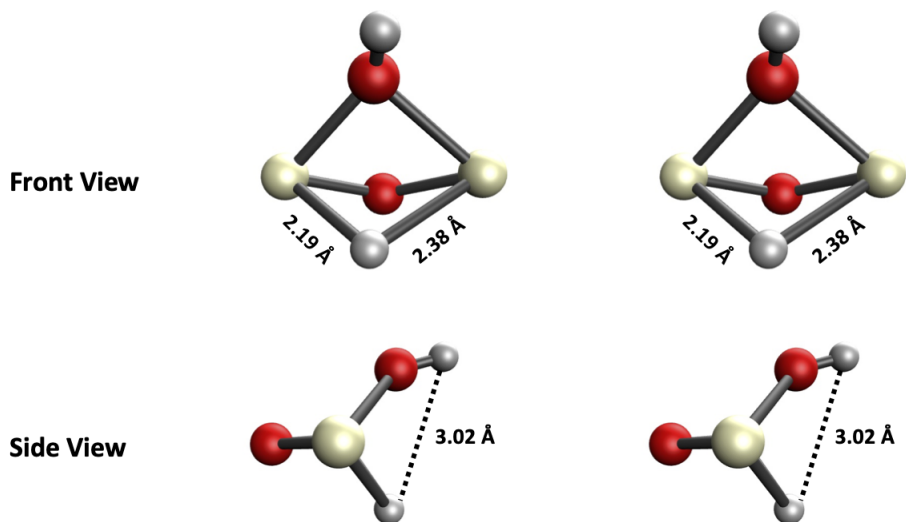
Figure 8: Front and side view of the geometry of structures quartet I-4 (left) and doublet I-2 (right).

(7.6 kcal/mol for the quartet and 6.5 kcal/mol for the doublet). In support of experimental interpretations,[47,48] these transition structures feature an electron rich hydroxide attracted by the electron-poor cerium centers resulting in diffuse multi-centered bonds involving the hydroxide and both cerium ions.
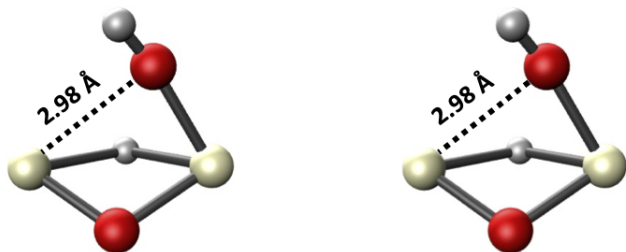

Figure 9: Structures of TS2-2 and TS2-4 that connect H-2 and H-4 to I-2 and I-4, respectively.

The final step of the mechanism involves H_2 production and formation of **C-4** or **C-2**. In both quartet and doublet pathways, this final step is quite exothermic. The energies of the separated products are 24.7 kcal/mol and 25.0 kcal/mol below the hydroxide/hydride bridge structures **I-4** and **I-2**, respectively. Relative to the initial quartet Ce_2O^-/water adduct, the reaction enthalpy for hydrogen gas evolution is -91.3 kcal/mol via the quartet pathway and -89.3 kcal/mol via the doublet pathway.
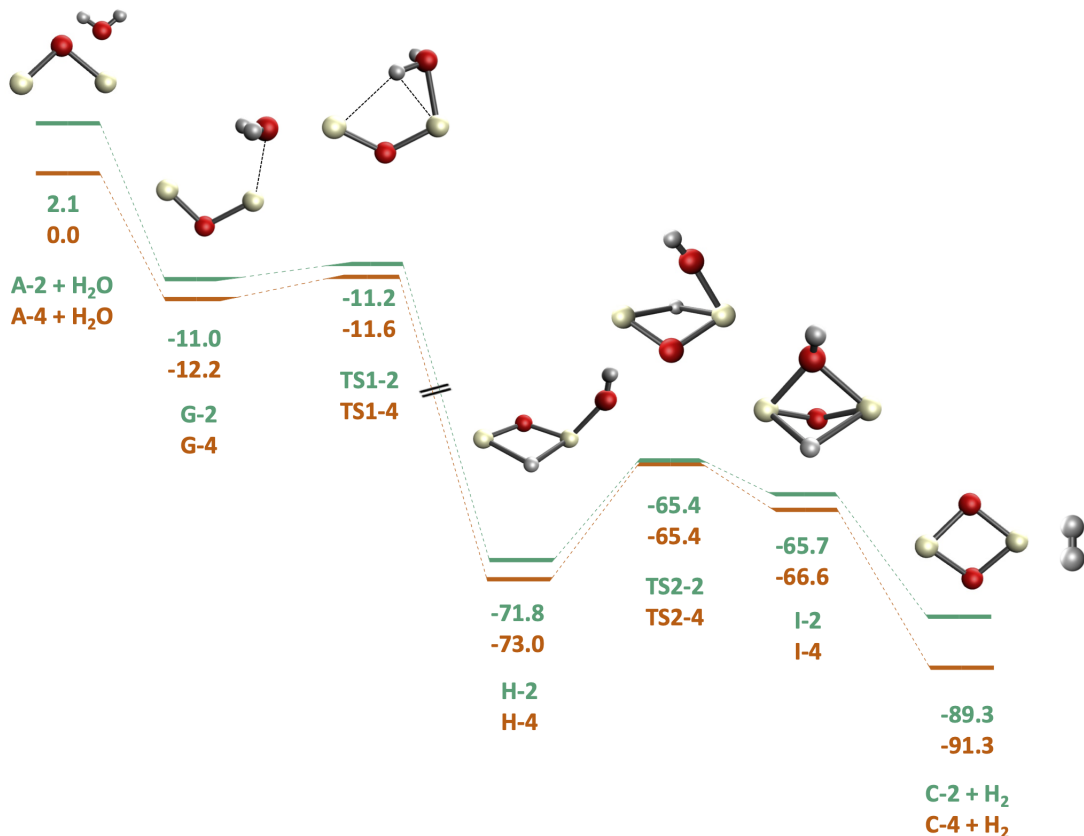
4 Discussion

Figure 10: Energy profile for the proposed $Ce_2O^- + H_2O \longrightarrow Ce_2O_2^- + H_2$ quartet (orange) and doublet (green) mechanisms

Figure 10 shows the full energy profile of the doublet (green) and quartet (orange) mechanistic routes. In both cases the overall reactions are barrierless, in agreement with the experimental data provided by Jarrold and coworkers.[47,48] The reaction can be summarized by four steps: (1) addition of water onto a cerium center of Ce_2O^-; (2) hydride transfer from water into a bridging position between the two cerium atoms; (3) bond formation between hydroxide and the far cerium atom; and (4) evolution of H_2. Importantly, the reaction profiles in Fig. 10 are based on calculations that implicitly treat scalar relativistic effects and ignore spin-orbit effects. These calculations predict energy gaps between 0.007 kcal/mol and 2.1 kcal/mol for the two lowest-energy pathways, which are related to one another by a single electron spin-flip. As such, both pathways are likely accessed due to the presence

of the lanthanide centers that will provide spin-orbit coupling between these two low-energy pathways.

The partially filled f-manifold in most lanthanide complexes lies close to the 5d and 6s orbitals of the lanthanide centers, yet it is non-bonding in nature and exhibits core-like behavior. Several studies have shown that the orbitals involved in chemical processes on lanthanides and lanthanide-based clusters involve 6s and 5p orbitals, while the occupation number of 4f orbitals remains intact.[46,47,69–72,76] While the cerium-based 6s orbitals have been previously determined to be the sites of electron detachments in various cerium and cerium suboxide clusters (including Ce_2O^- and $Ce_2O_2^-$), we notice here that both σ and σ^* orbitals retain all or most of their electron occupations as the reaction proceeds. This shows that σ and σ^* electrons are not the source of metal facilitated reduction of water. Instead, the electron source in the studied reaction is the set of singly occupied 5d orbitals. This observation is consistent with the reported experimental result that reaction of $Ce_2O_2^-$ with water yields H-radical rather than H_2. The reaction of water with Ce_2O^- depletes the metal centers of their d electrons and prevents further H_2 production.[17]

There are features of the Ce_2O^- catalyzed reaction that are different from reports published for transition metal oxide cluster analogues. Three such examples include tungsten oxide, molybdenum oxide, and mixed manganese-molybdenum oxides.[77–80] The overall reaction barriers for those cases is similar to the case reported in this work, but a key difference lies in the mode of addition of water to the clusters. Indeed, previous reports found that the initial steps of water addition occur via a concerted step involving simultaneous addition of hydroxide (from water) to the metal center and O−H formation at an oxo site. As discussed above, our calculations identified a different pathway for the reaction with cerium oxide that occurs via a two-step process: water adds to the cerium center to form structures **G-2** and **G-4** (Fig. 5), then the hydrogen transfers to a bridging position between the two cerium centers.

In the reaction of Mn_xMoO_y anions with water, both Mn and Mo are involved in the

initial cluster-water formation.[80] However, only the Mo center undergoes oxidation. In fact, the reactivity of the Mn_xMoO_y anion clusters with water depends on the oxidation state only of the molybdenum center. Once the Mo center reaches its highest oxidation state (VI), reaction with additional water molecules ends.

5   Conclusions

This work studied the reaction of water with Ce_2O^- clusters to produce $Ce_2O_2^-$ and H_2. Density functional theory calculations have been used to map out the full reaction pathway for hydrogen production. A thorough search for candidate intermediates and transition structures has shown that a key point in the progression of the reaction is the formation of successive bridging bonds that place the two hydrogen atoms in close proximity and eventually facilitates the production of H_2. We have also shown that it is energetically possible for both experimentally identified electronic states of Ce_2O^- to react with water and eliminate molecular hydrogen with low energy barriers relative to the starting materials. Finally, while the valence molecular orbitals of the studied cerium oxide clusters consist of 4f, 5d, and 6s metal-centered orbitals, an examination of the molecular orbitals of initial and final cerium oxide clusters clearly indicates that the metal 5d electrons provide the means for water reduction. This work provides new insight to the reactivity of small lanthanide-based clusters with water.

The reaction studied in this work provides insight to key driving features of an important reaction catalyzed by lanthanide suboxide clusters. Interestingly, experimental results have shown that variations in the lanthanide to oxide ratios in Ce_xO_y anion clusters is a dictating factor in the mode of reactivity of these clusters with water.[17] While the effect of this ratio on the reactivity with water is still not fully understood, our analysis using a molecular orbital approach shows that the reaction of Ce_2O^- clusters is driven by delocalized 5d electrons. A similar feature has been observed in a recent study[69] in which we showed the significant role

that lanthanide-based 5d orbitals play in the structure and bonding across the lanthanide hydroxide series. Studying cluster reactivity with varying ratios of lanthanides to oxides provides further understanding of the reactivity motifs of these clusters and insight for designing catalysts that can efficiently carry out efficient hydrogen gas production.

Acknowledgement

Funding Information

References

(1) Pettersson, L. G. M.; Henchman, R. H.; Nilsson, A. Water – The Most Anomalous Liquid. 2016.

(2) Speedy, R. J. Stability-limit conjecture. An interpretation of the properties of water. *J. Phys. Chem.* **1982**, *86*, 982–991.

(3) Poole, P. H.; Sciortino, F.; Essmann, U.; Stanley, H. E. Phase behaviour of metastable water. *Nature* **1992**, *360*, 324.

(4) Tanaka, H. Simple physical model of liquid water. *J. Chem. Phys.* **2000**, *112*, 799–809.

(5) Holten, V.; Anisimov, M. Entropy-driven liquid–liquid separation in supercooled water. *Sci. Rep.* **2012**, *2*, 713.

(6) Smith, J. D.; Cappa, C. D.; Wilson, K. R.; Cohen, R. C.; Geissler, P. L.; Saykally, R. J. Unified description of temperature-dependent hydrogen-bond rearrangements in liquid water. *Proc. Natl. Acad. Sci.* **2005**, *102*, 14171–14174.

(7) Liu, J.; Andino, R. S.; Miller, C. M.; Chen, X.; Wilkins, D. M.; Ceriotti, M.; Manolopoulos, D. E. A surface-specific isotope effect in mixtures of light and heavy water. *J. Phys. Chem. C* **2013**, *117*, 2944–2951.

(8) Medders, G. R.; Babin, V.; Paesani, F. Development of a "first-principles" water potential with flexible monomers. III. Liquid phase properties. *J. Chem. Theory Comput.* **2014**, *10*, 2906–2910.

(9) Bartók, A. P.; Payne, M. C.; Kondor, R.; Csányi, G. Gaussian approximation potentials: The accuracy of quantum mechanics, without the electrons. *Phys. Rev. Lett.* **2010**, *104*, 136403.

(10) Gillan, M. J.; Alfè, D.; Michaelides, A. Perspective: How good is DFT for water? *J. Chem. Phys.* **2016**, *144*, 130901.

(11) Gallo, P.; Amann-Winkel, K.; Angell, C. A.; Anisimov, M. A.; Caupin, F.; Chakravarty, C.; Lascaris, E.; Loerting, T.; Panagiotopoulos, A. Z.; Russo, J., et al. Water: A tale of two liquids. *Chem. Rev.* **2016**, *116*, 7463–7500.

(12) Hunter, B. M.; Gray, H. B.; Muller, A. M. Earth-abundant heterogeneous water oxidation catalysts. *Chem. Rev.* **2016**, *116*, 14120–14136.

(13) McEvoy, J. P.; Brudvig, G. W. Water-splitting chemistry of photosystem II. *Chem. Rev.* **2006**, *106*, 4455–4483.

(14) Walter, M. G.; Warren, E. L.; McKone, J. R.; Boettcher, S. W.; Mi, Q.; Santori, E. A.; Lewis, N. S. Solar water splitting cells. *Chem. Rev.* **2010**, *110*, 6446–6473.

(15) Tachibana, Y.; Vayssieres, L.; Durrant, J. R. Artificial photosynthesis for solar water-splitting. *Nat. Photonics* **2012**, *6*, 511.

(16) Kang, D.; Kim, T. W.; Kubota, S. R.; Cardiel, A. C.; Cha, H. G.; Choi, K.-S. Electrochemical synthesis of photoelectrodes and catalysts for use in solar water splitting. *Chem. Rev.* **2015**, *115*, 12839–12887.

(17) Felton, J. A.; Ray, M.; Waller, S. E.; Kafader, J. O.; Jarrold, C. C. $Ce_xO_y^-$ (x= 2–3) + D_2O Reactions: Stoichiometric Cluster Formation from Deuteroxide Decomposition and Anti-Arrhenius Behavior. *J. Phys. Chem. A* **2014**, *118*, 9960–9969.

(18) Graciani, J.; Márquez, A. M.; Plata, J. J.; Ortega, Y.; Hernández, N. C.; Meyer, A.; Zicovich-Wilson, C. M.; Sanz, J. F. Comparative study on the performance of hybrid DFT functionals in highly correlated oxides: The case of CeO_2 and Ce_2O_3. *J. Chem. Theory Comput.* **2010**, *7*, 56–65.

(19) Wu, X.-N.; Ding, X.-L.; Bai, S.-M.; Xu, B.; He, S.-G.; Shi, Q. Experimental and Theoretical Study of the Reactions between Cerium Oxide Cluster Anions and Carbon Monoxide: Size-Dependent Reactivity of $Ce_nO_{2n+1}^-$ (n= 1–21). *J. Phys. Chem. C* **2011**, *115*, 13329–13337.

(20) Nagata, T.; Miyajima, K.; Mafuné, F. Gold Atoms Supported on Gas-Phase Cerium Oxide Cluster Ions: Stable Stoichiometry and Reactivity with CO. *J. Phys. Chem. A* **2016**, *120*, 7624–7633.

(21) Nagata, T.; Miyajima, K.; Mafuné, F. Oxidation of nitric oxide on gas-phase cerium oxide clusters via reactant adsorption and product desorption processes. *J. Phys. Chem. A* **2015**, *119*, 10255–10263.

(22) Zhao, Y.-X.; Liu, Q.-Y.; Zhang, M.-Q.; He, S.-G. Reactions of metal cluster anions with inorganic and organic molecules in the gas phase. *Dalton Trans.* **2016**, *45*, 11471–11495.

(23) Idakiev, V.; Tabakova, T.; Tenchev, K.; Yuan, Z.-Y.; Ren, T.-Z.; Su, B.-L. Gold nanoparticles supported on ceria-modified mesoporous titania as highly active catalysts for low-temperature water-gas shift reaction. *Catal. Today* **2007**, *128*, 223–229.

(24) Fu, Q.; Saltsburg, H.; Flytzani-Stephanopoulos, M. Active nonmetallic Au and Pt species on ceria-based water-gas shift catalysts. *Science* **2003**, *301*, 935–938.

(25) Martınez-Arias, A.; Fernández-Garcıa, M.; Soria, J.; Conesa, J. Spectroscopic study of a Cu/CeO_2 catalyst subjected to redox treatments in carbon monoxide and oxygen. *J. Catal.* **1999**, *182*, 367–377.

(26) Takamura, H.; Kobayashi, T.; Kasahara, T.; Kamegawa, A.; Okada, M. Oxygen permeation and methane reforming properties of ceria-based composite membranes. *Journal of alloys and compounds* **2006**, *408*, 1084–1089.

(27) Fernández-Garcıa, M.; Martınez-Arias, A.; Salamanca, L.; Coronado, J.; Anderson, J.; Conesa, J.; Soria, J. Influence of ceria on Pd activity for the CO $+O_2$ reaction. *J. Catal.* **1999**, *187*, 474–485.

(28) Esposito, V.; Traversa, E. Design of electroceramics for solid oxides fuel cell applications: playing with ceria. *J. Am. Ceram. Soc.* **2008**, *91*, 1037–1051.

(29) Aneggi, E.; Boaro, M.; de Leitenburg, C.; Dolcetti, G.; Trovarelli, A. Insights into the redox properties of ceria-based oxides and their implications in catalysis. *J. Alloys Compd.* **2006**, *408*, 1096–1102.

(30) Gorte, R. J. Ceria in catalysis: From automotive applications to the water–gas shift reaction. *AIChE J.* **2010**, *56*, 1126–1135.

(31) Saraf, L.; Wang, C. M.; Shutthanandan, V.; Zhang, Y.; Marina, O.; Baer, D. R.; Thevuthasan, S.; Nachimuthu, P.; Lindle, D. W. Oxygen transport studies in nanocrystalline ceria films. *J. Mater. Res.* **2005**, *20*, 1295–1299.

(32) Montini, T.; Melchionna, M.; Monai, M.; Fornasiero, P. Fundamentals and catalytic applications of CeO_2-based materials. *Chem. Rev.* **2016**, *116*, 5987–6041.

(33) Li, Y.; Fu, Q.; Flytzani-Stephanopoulos, M. Low-temperature water-gas shift reaction over Cu-and Ni-loaded cerium oxide catalysts. *Appl. Catal., B* **2000**, *27*, 179–191.

(34) Bunluesin, T.; Gorte, R.; Graham, G. Studies of the water-gas-shift reaction on ceria-supported Pt, Pd, and Rh: implications for oxygen-storage properties. *Appl. Catal., B* **1998**, *15*, 107–114.

(35) Luengnaruemitchai, A.; Osuwan, S.; Gulari, E. Comparative studies of low-temperature water–gas shift reaction over Pt/CeO_2, Au/CeO_2, and Au/Fe_2O_3 catalysts. *Catal. Commun.* **2003**, *4*, 215–221.

(36) Biswas, S.; Husek, J.; Londo, S.; Baker, L. R. Highly localized charge transfer excitons in metal oxide semiconductors. *Nano Lett.* **2018**, *18*, 1228–1233.

(37) Zhou, R.; Yang, Y.; Pande, S.; Qu, B.; Li, D.; Zeng, X. C. Reaction mechanism between small-sized Ce clusters and water molecules: an ab initio investigation on Ce_n + H_2O. *Phys. Chem. Chem. Phys.* **2019**, *21*, 4006–4014.

(38) Zhou, R.; Ma, S.; Yang, Y.; Li, D.; Qu, B.; Zeng, X. C. Reaction mechanism between small-sized Ce clusters and water molecules II: an ab initio investigation on Ce_n (n= 1–3)+ m H_2O (m= 2–6). *Phys. Chem. Chem. Phys.* **2019**, *21*, 8945–8955.

(39) Li, Y.; Gong, Y.; Zhou, X.; Su, J.; Li, J.; Zhou, M. Infrared spectroscopic and theoretical study of the reactions of cerium atoms with methanol in solid argon. *J. Mol. Spectrosc.* **2015**, *310*, 50–56.

(40) Xu, B.; Shi, P.; Huang, T.; Wang, X. Hydrogen-bridge $Si(\mu-H)_3CeH$ and inserted H_3SiCeH molecules: Matrix infrared spectra and DFT calculations for reaction products of silane with Ce atoms. *J. Mol. Struct.* **2017**, *1146*, 692–702.

(41) Wang, X.; Andrews, L.; Fang, Z.; Thanthiriwatte, K. S.; Chen, M.; Dixon, D. A. Properties of Lanthanide Hydroxide Molecules Produced in Reactions of Lanthanide Atoms with H_2O_2 and $H_2+ O_2$ Mixtures: Roles of the +I, +II, +III, and +IV Oxidation States. *J. Phys. Chem. A* **2017**, *121*, 1779–1796.

(42) Fang, Z.; Thanthiriwatte, K. S.; Dixon, D. A.; Andrews, L.; Wang, X. Properties of cerium hydroxides from matrix infrared spectra and electronic structure calculations. *Inorg. Chem.* **2016**, *55*, 1702–1714.

(43) Pu, Z.; Yu, W.; Roy, S. K.; Li, C.; Ao, B.; Liu, T.; Shuai, M.; Wang, X. Insights into the enhanced CeN triple bond in the HCeN molecule. *Phys. Chem. Chem. Phys.* **2017**, *19*, 8216–8222.

(44) Mikulas, T. C.; Chen, M.; Fang, Z.; Peterson, K. A.; Andrews, L.; Dixon, D. A. Structures and Properties of the Products of the Reaction of Lanthanide Atoms with H_2O: Dominance of the +II Oxidation State. *J. Phys. Chem. A* **2016**, *120*, 793–804.

(45) Kafader, J. O.; Ray, M.; Jarrold, C. C. Low-lying electronic structure of EuH, EuOH, and EuO neutrals and anions determined by anion photoelectron spectroscopy and DFT calculations. *J. Chem. Phys.* **2015**, *143*, 034305.

(46) Kafader, J. O.; Ray, M.; Jarrold, C. C. Photoelectron spectrum of PrO^-. *J. Chem. Phys.* **2015**, *143*, 064305.

(47) Kafader, J. O.; Topolski, J. E.; Jarrold, C. C. Molecular and electronic structures of cerium and cerium suboxide clusters. *J. Chem. Phys.* **2016**, *145*, 154306.

(48) Topolski, J.; Kafader, J.; Ray, M.; Jarrold, C. Elucidating cerium $+ H_2O$ reactivity through electronic structure: A combined PES and DFT study. *J. Mol. Spectrosc.* **2017**, *336*, 1–11.

(49) Ray, M.; Kafader, J. O.; Topolski, J. E.; Jarrold, C. C. Mixed cerium-platinum oxides: Electronic structure of $[CeO]Pt_n$ (n= 1, 2) and $[CeO_2]Pt$ complex anions and neutrals. *J. Chem. Phys.* **2016**, *145*, 044317.

(50) Topolski, J. E.; Kafader, J. O.; Jarrold, C. C. Ce in the +4 oxidation state: Anion photoelectron spectroscopy and photodissociation of small $Ce_xO_yH_z^-$ molecules. *J. Chem. Phys.* **2017**, *147*, 104303.

(51) Topolski, J. E.; Kafader, J. O.; Marrero-Colon, V.; Iyengar, S. S.; Hratchian, H. P.; Jarrold, C. C. Exotic electronic structures of $Sm_xCe_{3-x}O_y$ (x= 0-3; y= 2-4) clusters and the effect of high neutral density of low-lying states on photodetachment transition intensities. *J. Chem. Phys.* **2018**, *149*, 054305.

(52) Frisch, M. J.; Trucks, G. W.; Schlegel, H. B.; Scuseria, G. E.; Robb, M. A.; Cheeseman, J. R.; Scalmani, G.; Barone, V.; Petersson, G. A.; Nakatsuji, H.; Li, X.; Caricato, M.; Marenich, A. V.; Bloino, J.; Janesko, B. G.; Gomperts, R.; Mennucci, B.; Hratchian, H. P.; Ortiz, J. V.; Izmaylov, A. F.; Sonnenberg, J. L.; Williams-Young, D.; Ding, F.; Lipparini, F.; Egidi, F.; Goings, J.; Peng, B.; Petrone, A.; Henderson, T.; Ranasinghe, D.; Zakrzewski, V. G.; Gao, J.; Rega, N.; Zheng, G.; Liang, W.; Hada, M.; Ehara, M.; Toyota, K.; Fukuda, R.; Hasegawa, J.; Ishida, M.; Nakajima, T.; Honda, Y.; Kitao, O.; Nakai, H.; Vreven, T.; Throssell, K.; Montgomery, J. A., Jr.; Peralta, J. E.; Ogliaro, F.; Bearpark, M. J.; Heyd, J. J.; Brothers, E. N.; Kudin, K. N.; Staroverov, V. N.; Keith, T. A.; Kobayashi, R.; Normand, J.; Raghavachari, K.; Rendell, A. P.; Burant, J. C.; Iyengar, S. S.; Tomasi, J.; Cossi, M.; Millam, J. M.; Klene, M.; Adamo, C.; Cammi, R.; Ochterski, J. W.; Martin, R. L.; Morokuma, K.; Farkas, O.; Foresman, J. B.; Fox, D. J. Gaussian Development Version Revision J.04+. 2019; Gaussian Inc. Wallingford CT.

(53) Perdew, J. P.; Chevary, J. A.; Vosko, S. H.; Jackson, K. A.; Pederson, M. R.; Singh, D. J.; Fiolhais, C. Atoms, molecules, solids, and surfaces: Applications of the

generalized gradient approximation for exchange and correlation. *Phys. Rev. B* **1992**, *46*, 6671.

(54) Perdew, J. P.; Wang, Y. Accurate and simple analytic representation of the electron-gas correlation energy. *Phys. Rev. B* **1992**, *45*, 13244.

(55) Becke, A. D. Density-functional thermochemistry. IV. A new dynamical correlation functional and implications for exact-exchange mixing. *J. Chem. Phys.* **1996**, *104*, 1040–1046.

(56) Becke, A. D. Density-functional thermochemistry. III. The role of exact exchange. *J. Chem. Phys.* **1993**, *98*, 5648–5652.

(57) Becke, A. D. Density-functional thermochemistry. II. The effect of the Perdew–Wang generalized-gradient correlation correction. *J. Chem. Phys.* **1992**, *97*, 9173–9177.

(58) Pople, J.; Nesbet, R. Self-consistent orbitals for radicals. *J. Chem. Phys.* **1954**, *22*, 571–572.

(59) Pople, J. A.; Gill, P. M.; Handy, N. C. Spin-unrestricted character of Kohn-Sham orbitals for open-shell systems. *International Journal of Quantum Chemistry* **1995**, *56*, 303–305.

(60) Bauernschmitt, R.; Ahlrichs, R. Stability analysis for solutions of the closed shell Kohn–Sham equation. *J. Chem. Phys.* **1996**, *104*, 9047–9052.

(61) Seeger, R.; Pople, J. A. Self-consistent molecular orbital methods. XVIII. Constraints and stability in Hartree–Fock theory. *J. Chem. Phys.* **1977**, *66*, 3045–3050.

(62) Sonnenberg, J. L.; Schlegel, H. B.; Hratchian, H. P. Spin contamination in inorganic chemistry calculations. *Encyclopedia of Inorganic and Bioinorganic Chemistry* **2011**,

(63) Cao, X.; Dolg, M. Valence basis sets for relativistic energy-consistent small-core lanthanide pseudopotentials. *J. Chem. Phys.* **2001**, *115*, 7348–7355.

(64) Kendall, R. A.; Dunning Jr, T. H.; Harrison, R. J. Electron affinities of the first-row atoms revisited. Systematic basis sets and wave functions. *J. Chem. Phys.* **1992**, *96*, 6796–6806.

(65) Papajak, E.; Zheng, J.; Xu, X.; Leverentz, H. R.; Truhlar, D. G. Perspectives on basis sets beautiful: seasonal plantings of diffuse basis functions. *J. Chem. Theory Comput.* **2011**, *7*, 3027–3034.

(66) Hratchian, H. P.; Schlegel, H. B. *Theory and Applications of Computational Chemistry*; Elsevier, 2005; pp 195–249.

(67) Hratchian, H. P.; Schlegel, H. B. Accurate reaction paths using a Hessian based predictor–corrector integrator. *J. Chem. Phys.* **2004**, *120*, 9918–9924.

(68) Hratchian, H.; Schlegel, H. Using Hessian updating to increase the efficiency of a Hessian based predictor-corrector reaction path following method. *J. Chem. Theory Comput.* **2005**, *1*, 61–69.

(69) Harb, H.; Thompson, L. M.; Hratchian, H. P. On the linear geometry of lanthanide hydroxide (Ln-OH, Ln= La–Lu). *Phys. Chem. Chem. Phys.* **2019**, *21*, 21890–21897.

(70) Mason, J. L.; Harb, H.; Topolski, J. E.; Hratchian, H. P.; Jarrold, C. C. Exceptionally Complex Electronic Structures of Lanthanide Oxides and Small Molecules. *Acc. Chem. Res.* **2019**, *52*, 3265–3273.

(71) Maron, L.; Eisenstein, O. Do f Electrons Play a Role in the Lanthanide- Ligand Bonds? A DFT Study of $Ln(NR_2)_3$; R= H, SiH_3. *J. Phys. Chem. A* **2000**, *104*, 7140–7143.

(72) Eisenstein, O.; Maron, L. DFT studies of some structures and reactions of lanthanides complexes. *J. Organomet. Chem.* **2002**, *647*, 190–197.

(73) Mason, J. L.; Harb, H.; Abou Taka, A.; McMahon, A.; Huizenga, C. D.; Corzo, H. H.; Hratchian, H. P.; Jarrold, C. C. Photoelectron Spectra of $Gd_2O_2^-$ and Non-Monotonic

Photon-Energy Dependent Variations in Populations of Close-Lying Neutral States. *ChemRxiv* **2020**, *2020*, 10.26434/chemrxiv.13237307.

(74) Mason, J. L.; Topolski, J. E.; Ewigleben, J.; Iyengar, S. S.; Jarrold, C. C. Photoelectrons Are Not Always Quite Free. *J. Phys. Chem. Lett.* **2018**, *10*, 144–149.

(75) McMahon, A. J.; Jarrold, C. C. Using anion photoelectron spectroscopy of cluster models to gain insights into mechanisms of catalyst-mediated H_2 production from water. *Phys. Chem. Chem. Phys.* **2020**,

(76) Roos, B. O.; Pyykkö, P. Bonding Trends in Molecular Compounds of Lanthanides: The Double-Bonded Carbene Cations $LnCH_2^+$ (Ln= Sc, Y, La–Lu). *Chem. - Eur. J.* **2010**, *16*, 270–275.

(77) Mayhall, N. J.; Rothgeb, D. W.; Hossain, E.; Jarrold, C. C.; Raghavachari, K. Water reactivity with tungsten oxides: H_2 production and kinetic traps. *J. Chem. Phys.* **2009**, *131*, 144302.

(78) Mayhall, N. J.; Raghavachari, K. Two Methanes are Better than One: A Density Functional Theory Study of the Reactions of $Mo_2O_y^-$ (y= 2- 5) with Methane. *J. Phys. Chem. A* **2007**, *111*, 8211–8217.

(79) Yoder, B. L.; Maze, J. T.; Raghavachari, K.; Jarrold, C. C. Structures of $Mo_2O_y^-$ and Mo_2O_y (y= 2, 3, and 4) studied by anion photoelectron spectroscopy and density functional theory calculations. *J. Chem. Phys.* **2005**, *122*, 094313.

(80) Mason, J. L.; Gupta, A. K.; McMahon, A. J.; Folluo, C. N.; Raghavachari, K.; Jarrold, C. C. The striking influence of oxophilicity differences in heterometallic Mo–Mn oxide cluster reactions with water. *J. Chem. Phys.* **2020**, *152*, 054301.

Graphical TOC Entry
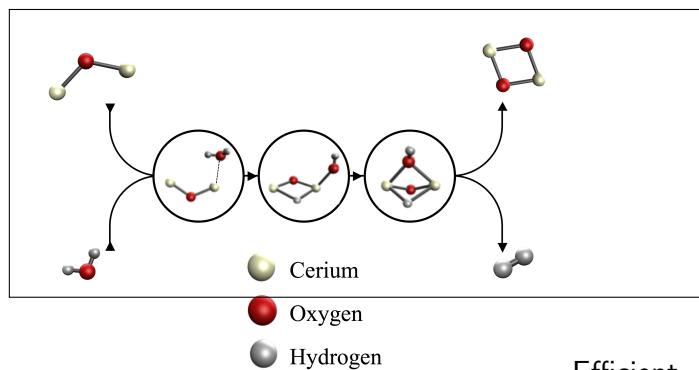
Efficient hydrogen evolution from water by Ce_2O^- is driven by the cerium 5d, rather than 6s, electrons.